Wood Hole-Damage Detection and Classification via Contact Ultrasonic Testing

Mohsen Mousavi[a], Amir H Gandomi *[a]

[a]*Faculty of Engineering and IT, University of Technology Sydney, Ultimo, NSW 2007, Australia.*

Abstract

Damage detection in wood materials has numerous applications in different industries, such as construction and forestry. Wood is generally a complex medium due to its orthotropic and random properties, which increases the difficulty of non-destructive damage testing. However, machine learning algorithms can be employed to overcome this problem. In this paper, hole-defect classification problems of two common types of wood materials, namely hard (marbau) and soft (pine) wood, are studied using a naive Bayes classification technique. To this end, the results of contact ultrasonic tests conducted on these types of woods in different directions, i.e. tangential and radial to the growth rings of wood, were investigated. The various states of the intact, small defect, and large defect of each type of wood were considered in the testing regime. It is known that contact ultrasonic tests are highly sensitive to different aspects of the test, such as the amount of couplant gel applied to surfaces, the amount of pressure applied to the transducer and receiver, and misalignment of the transducer and receiver. Therefore, 50 replicates of each test were implemented. First, an advanced signal decomposition algorithm termed Variational Mode Decomposition (VMD) was exploited to derive some features from the recorded ultrasonic signals. Then, the derived features were used in a set of classification problems using a naive Bayes classifier to classify the damage state of the specimens. Different types of naive Bayes classifiers, namely Gaussian and kernel, along with combinations of different types of features were employed to improve the results, ultimately achieving nearly 100% 10-fold cross-validation accuracy in all cases individually. However, when cases from different types of wood and direction of the tests were mixed, 93.6% 10-fold cross-validation accuracy was achieved for the classification problem based on the health state of the cases, using kernel naive Bayes classifier and a mixture of two types of features.

Keywords: `Ultrasonics, Variational Mode Decomposition, Naive Bayse Classifier, Nondestructive testing, Wood, Damage sensitive feature`

Email addresses: `mohsen.mousavi@uts.edu.au` (Mohsen Mousavi), `gandomi@uts.edu.au` (Amir H Gandomi *)

1. Introduction

Wood is an effective material for construction due to its good heat and electrical insulation, workability, among other useful properties [1, 2]. For instance, in Australia, more than 80% of power utility poles, roughly more than 5 million poles in total, are made from wood [3, 4].

Wood may be described as an orthotropic material, which means that its mechanical properties vary in different directions [5]. Therefore, independent mechanical properties are usually expected in three mutually perpendicular axes, i.e. longitudinal (parallel to the fiber/grain), radial (normal to the growth rings), and tangential (tangent to the growth rings) [6]. However, this diversity of mechanical properties can vary from one type of wood to another due to the change of the microfibril angle [7]. These mechanical properties can be identified using different techniques, such as static tests [8], near-infrared (NIR) spectroscopy [9], image processing [10], and acoustic measurements [11].

However, wood materials may deteriorate during production and/or while in-service. The former can happen when standing trees are not pruned and, therefore, undergo a process of natural self-pruning. The latter occurs due to either biological (such as decay, fungi, and termites) or physical (climatic such as rain and sun) processes [12]. Therefore, detection techniques for assessing wood quality in different industries have attracted more research interest. This includes wood damage monitoring for mechanised harvesting [13], damage detection of in-service wooden poles [3, 14, 15, 16, 17], preservation of wooden architectural heritage [18, 19, 20], as well as forest quality assessment, which is an important research field in forestry [21, 22].

Over the past decade, many different non-destructive damage testing (NDT) techniques have been developed for wood material assessment. These techniques generally have two key components: 1) a sensing technology used for conducting a nondestructive damage testing on wood structures, and 2) a damage detection or classification strategy to derive information about the health condition of the wood materials from the recorded signals.

Different sensing technologies have also been employed to this end, such as ultrasonics [23], radiography [24] and thermography [25]. Among these, ultrasonic testing seems to be the most promising and widely used approach since it is less intrusive and less expensive [26] compared to other methods. Moreover, ultrasonic waves are highly sensitive to wood mechanical properties and defects [27].

Ultrasonic techniques have been widely used for the evaluation of wood materials [28, 29, 30, 31, 32, 33]. Among such studies, the evaluation of mechanical properties of wood with artificial deterioration has received great interest from researchers [12, 29, 34, 35]. Ultrasonic devices can be classified into two main categories: contact and non-contact devices. The non-contact

ultrasonic devices include electromagnet ultrasonics (EU) [36], laser ultrasonics (LU) [37], and air-coupled ultrasonics (ACU) [38, 39, 40, 41]. Although the use of non-contact ultrasonics for NDT has been reported widely in the literature, there are some limitations in terms of their application. For instance, EU devices do not perform well in non-conductive mediums, and LU devices are relatively expensive. It is known that ACU devices are effective when used for evaluation of low density materials, like paper, wood, and carbon-reinforced composites due to the smaller impedance difference between such materials and air [40]. However, the quality of ACU signals is usually poor, thus further demanding more advanced signal processing techniques to process signals obtained from ACU tests [39]. Therefore, the application of contact ultrasonic devices still seems promising despite some existing challenges. For instance, a couplant gel needs to be employed to fill the gap between the transducer/receiver and surface of the wooden section to ensure proper transmissibility of the ultrasonic waves into the wood material. Also, any misalignment or vibration of the transmitter or receiver can affect the quality of measurements.

This work demonstrates the possibility of using contact ultrasonics for damage evaluation of wood materials, namely soft (pine) and hard (marbau) timbers. Damage was artificially introduced to the specimens in both radial and tangential directions to the growth rings of wood. Two types of hole damage were drilled into the specimens to synthesise small and large defects. A contact ultrasonic device was used for 50 replicate tests on each specimen. An advanced signal processing approach termed Variational Mode Decomposition (VMD) was then used to derive some features from the recorded signals. These features were subsequently fed into a naive Bayes classifier to solve some supervised damage classification problems. As such, further organisation of this paper is as follows:

In Chapter 2, the procedure of the experimental tests are explained. Then, Chapter 3 presents the theory of VMD and how it can be used to derive features from the recorded ultrasonic signals. Since VMD is a parametric decomposition algorithm, the procedure of specifying an appropriate value to each parameter for the purpose of this paper is explained. In Chapter 4, the theory of the naive Bayes classifier is described. Chapter 5 provides a detailed discussion of the obtained results from solving the classification problems using different types of features. Finally, some concluding remarks and perspectives for future work are drawn in Chapter 6.

2. Experimental set-up and measurements

The two types of wood materials studied in this study include soft (pine) and hard (merbau) wood. A total of six specimens of each type was selected for testing, where the size of each specimen was $300 \times 90 \times 90$ mm^3. The testing procedure was performed on each specimen in

Table 1: The number of test samples collected from different types of ultrasonic tests.

Radial test (tangential defect)		
Defect type	**Softwood**	**Hardwood**
Intact	300	300
Small tangential defect	150	150
Large tangential defect	150	150
Tangential test (radial defect)		
Defect type	**Softwood**	**Hardwood**
Intact	300	300
Small radial defect	150	150
Large radial defect	150	150

three phases: (1) intact, (2) small defect, and (3) large defect states of the specimens. In phase (1), all six specimens of each type were initially tested in both radial and tangential directions. In phase (2), a 6-mm small hole (roughly 7% of the cross section of specimens) was drilled through the tangential direction of three out of six specimens to simulate a small defect, and then the specimens were tested along their radial direction (perpendicular to the line of defect) (Figure 1c). For the remaining three specimens, a small hole was drilled with the same size through their radial direction and tested through their tangential direction (Figure 1d). In phase (3), for all defective specimens from stage (2), a larger 13-mm hole (roughly 14% of the cross section of specimens) was drilled, and the same procedure of testing in phase (3) was repeated.

The testing device was a Pundit PL200, as shown in Figure 1b. According to the device manual [42], 54-kHZ ultrasonic transducers are more suitable, than other alternatives such as 250-kHz transducers, for testing wood materials. Therefore, the 54-kHz transducer was employed to transmit a sinc-like probing P-wave (compression wave). The sampling frequency was set at 10 MHz on the device at the receiver side to provide enough resolution in the frequency domain. The readers are referred to [43] for further details. In order to ensure a proper contact, a couplant gel (Proceq Ultraschall-Koppelpaste) was used to fill the gap between the surface of the transducer and receiver and the specimens. However, there were uncertainties regarding the amount of the gel to-be used and the amount of pressure to-be applied to the transducer and receiver by hand. To address this issue, 50 replicates of each ultrasonic test were conducted in each case. Table 1 shows the number of tests conducted on the specimens of different types and health conditions. Next, we explain how some damage sensitive features (DSFs) can be derived from each measurement using an advanced signal decomposition technique, called Variational

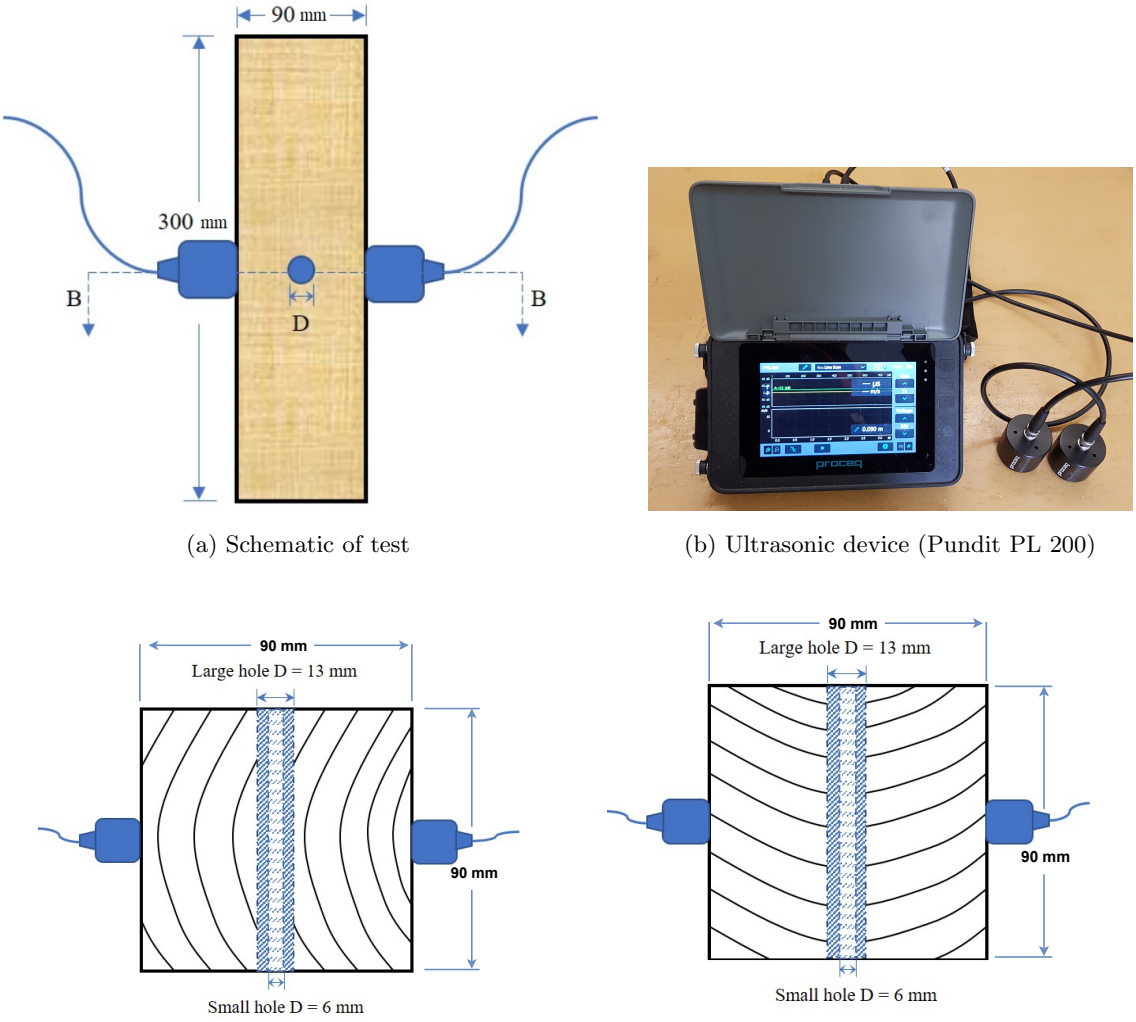

(a) Schematic of test

(b) Ultrasonic device (Pundit PL 200)

(c) Radial test (B-B)

(d) Tangential test (B-B)

Figure 1: Ultrasonic test experimental set-up [43].

Mode Decomposition (VMD).

3. Feature extraction using Variational Mode Decomposition

The raw recorded ultrasonic signals need to be preprocessed to derive some DSFs to be fed into the classification problems. To that end, VMD was used considering the fact that wood is a random medium and there are many nonlinear effects in the recorded ultrasonic signals due to the interaction between the ultrasonic waves and the wood grains. A discussion on the basic theories of VMD is subsequently provided to clarify its application for feature extraction.

VMD is an advanced signal decomposition algorithm that is used to decompose a non-linear non-stationary signal into its oscillatory modes, which are termed Intrinsic Mode Functions

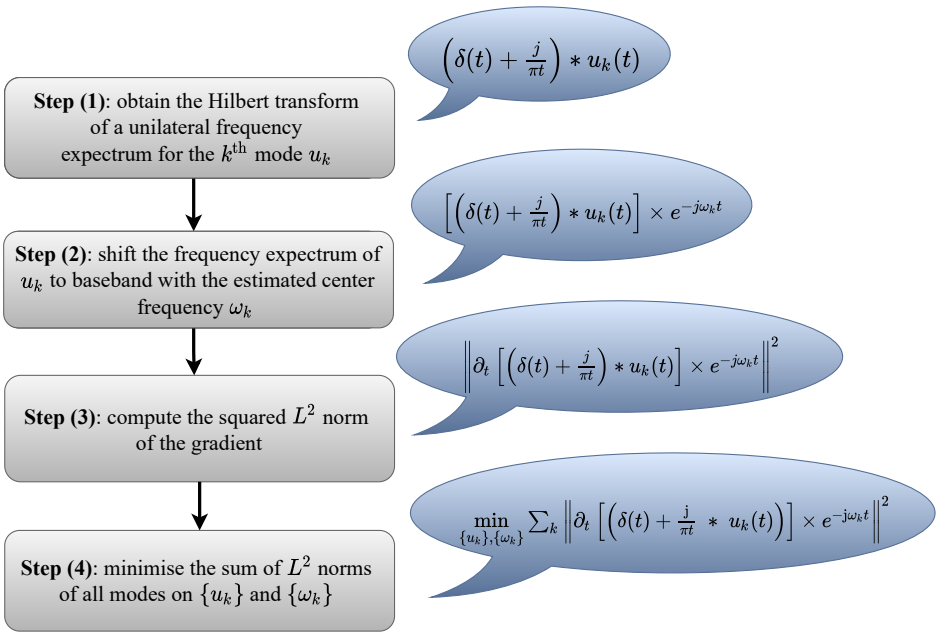

Figure 2: The general scheme of the VMD applied to a signal $S(t)$ under the constraint of $S(t) = \Sigma_k\, u_k(t)$.

(IMF) [44]. Each IMF is a frequency and/or amplitude modulated signal in the form of

$$u_k(t) = A_k(t)\cos(\phi_k(t)) \tag{1}$$

where $A_k(t)$ and $\phi_k(t)$ are the time-dependent amplitude and phase of the k^{th} IMF, respectively. VMD is a variational optimisation problem, which decomposes a given signal $S(t)$ into K IMFs $\{u_k\} = \{u_1, u_2, ..., u_K\}$, the sum of which constructs the original signal minus some noise, depending on the settings. Each IMF is narrow-band and, therefore, can be considered mono-component. As such, the instantaneous frequency of an IMF varies slightly around its center frequency ω_k where $k \in \{1, 2, \ldots, K\}$. The aforementioned variational optimisation problem of VMD is written as:

$$\min_{\{u_k\}\ \&\ \{\omega_k\}} \sum_k \left\| \partial_t \left[\left(\delta(t) + \frac{j}{\pi t} * u_k(t)\right) e^{-j\omega_k t} \right] \right\|^2; \quad s.t. \quad S(t) = \sum_k u_k(t) \tag{2}$$

where, in (2), $*$ is the convolution operator, and j is the imaginary unit. Figure 2 shows the overall scheme of the VMD that leads to obtaining (2). The solution to the above minimisation problem is the saddle point of the augmented Lagrangian in a sequence of iterative sub-optimizations called the alternate direction method of multipliers (ADMM) [44]. As such, VMD is a parametric decomposition algorithm, meaning that some parameters need to be specified prior to decomposition. These include:

1. The number of IMFS K, which determines how many modes the signal will be decomposed into. Later, this paper will demonstrate that the number of decomposition plays an important role in the classification problem.

2. The quadratic penalty term α, which is a denoising factor. The larger the α, the less the amount of the noise admitted to the decomposition process. As such, for a large α, the exact reconstruction is not possible due to the denoising effect.
3. Time step τ, which determines how quickly the Lagrangian multiplier accumulates the reconstruction error. In case the exact reconstruction is intended, one can set τ to a small number like 0.1, as suggested by the proposers of VMD [45]. Otherwise, one can set τ to zero when the reconstruction is not strictly enforced, but is encouraged in least-squares sense. Since a lowpass filter is used for denoising in this paper, τ is set to 0.1. Therefore, regardless of the value of α, denoising will not occur during the decomposition process, although, in this paper, a small value of $\alpha = 10$ was considered.
4. The tolerance parameter ϵ, which controls the convergence of the algorithm, is set to 10^{-5} in this paper. Selecting a smaller value, say $\epsilon = 10^{-}7$, only increased the time of decomposition while not having any further improvement effect on the decomposition results.
5. Initialisation center frequency of IMFs *init*, which initialises $\{\omega_k\}$ and can be either zero ($init = 0$), uniform ($init = 1$), or random ($init = 2$). It has been reported that the way of initialising center frequencies has little effect on the decomposition results [46]. Therefore, in this paper, the initial guess for ω is specified to zero, i.e. $init = 0$.
6. Deriving a DC component DC, which determines whether or not the first mode is set and kept at DC (zero frequency). Since the center frequency of IMFS is taken as features in this paper, it is important that DC be set to zero (false) due to the fact that no DC component (an IMF with zero center frequency) should be extracted from ultrasonic signals.[1]

Herein, all signals were first normalized and passed through a low-pass filter, then decomposed into K IMFs. The center frequency of IMFs were taken as the features in this work. The naive Bayes classifier was used to solve the classification problem using the derived features based on the labeled training sets. Further details will be discussed, following a brief presentation of the background theory of the naive Bayes classification technique.

4. Feature classification using naive Bayes Classifier

Naive Bayes is a Bayesian classifier that assigns the most likely class C to a given example described by its features $\boldsymbol{X} = (x_1, x_2, \ldots, x_n)$, assuming that features are independent for

[1]Note that the naive Bayes classifier fits a probability distribution to each feature across all observations. However, having identical zero center frequencies (features) will contradict this.

a given class. This assumption can be stated as $P(\boldsymbol{X}|\ C) = \prod_{j=1}^{n} P(x_j|\ C)$. Despite this unrealistic assumption, the resulting classifier is remarkably successful in practice. However, this assumption is compatible with the features derived from VMD as it decomposes a signal into some quasi-orthogonal components. Therefore, relatively independent center frequencies are derived for the components. The basic theory of the naive Bayes classification technique is subsequently discussed.

Consider $\boldsymbol{X}$ to be vector of features, where each feature x_i takes a value in its domain D_i. Therefore, the set of all feature vectors can be shown as $\Omega = D_1 \times D_2 \times \cdots \times D_n$. Take m as the number of classes and C as an unobserved random variable denoting the class to which each feature $\boldsymbol{X}$ is assigned. As such, C can take a value in $\{0, 1, 2, \ldots, m-1\}$. Accordingly, function $g : \Omega \longrightarrow \{0, 1, 2, \ldots, m-1\}$ is a concept to be learned, where $g(\boldsymbol{X}) = C$. There can be two types of concepts: deterministic and undeterministic. As such, deterministic g is a noise-free concept that always assigns the same class to a given feature, although it can be noisy in general and, therefore, random.

By applying the Bayes rule, one can obtain *a posteriori* probability of a class $C = i$ given $\boldsymbol{X}$ as:

$$P(C = i|\ \boldsymbol{X}) = \frac{P(\boldsymbol{X}|\ C = i)\ P(C = i)}{P(\boldsymbol{X})}. \tag{3}$$

where $P(C = i)$ and $P(C = i|\ \boldsymbol{X})$ are *a priori* and *a posteriori* probabilities of the i^{th} class given the set of features $\boldsymbol{X}$, respectively. $P(\boldsymbol{X}|\ C = i)$ is the likelihood of feature vector $\boldsymbol{X}$ representing the i^{th} class, and $P(\boldsymbol{X})$ is the probability of predictors regardless of the hypothesis and is identical for all classes. Therefore, according to the law of total probability, the denominator of (3) is effectively identical for all hypotheses and can be ignored. As such, the Bayes discriminant function $f_i^*(\boldsymbol{X})$ for a given class $i \in \{0, 1, 2, \ldots, m-1\}$ is defined as:

$$f_i^*(\boldsymbol{X}) = P(\boldsymbol{X}|\ C = i)\ P(C = i) \tag{4}$$

The Bayes classifier for a particular class i is then the discriminant function $h^*(x)$ that maximizes (4); and therefore:

$$h^*(\boldsymbol{X}) = \arg\max_i\ P(\boldsymbol{X}|\ C = i)\ P(C = i) \tag{5}$$

which finds the maximum *a posteriori* probability (MAP) for given $\boldsymbol{X}$. Since the direct estimation of $P(\boldsymbol{X}|\ C = i)$ in (5) is usually hard, the *naive Bayes* classifier benefits from the assumption that the features are independent. As such, the naive Bayes classifier $NB(x)$ is defined by discriminant functions f_i^{NB} as:

$$f_i^{NB}(\boldsymbol{X}) = \prod_{j=1}^{n}\ P(x_j|\ C = i)\ P(C = i) \tag{6}$$

Different probability distribution functions can be used to represent the distribution of predictors (features), the most common of which is the Gaussian distribution function. In this work, we applied two types of naive Bayes classifiers, namely Gaussian and kernel naive Bayes. To this end, we first started with the Gaussian naive Bayes classifier to try to achieve the best results for all cases. We further demonstrate why the simple naive Bayes may not be applicable to some cases, and therefore, the kernel naive Bayes should be used instead.

Further details about the background theory of the naive Bayes classification technique can be found in [47].

5. Experimental results and discussions

5.1. Using center frequency of IMFs as feature

All signals were passed through a lowpass filter with a cutoff frequency of 300 kHz which is an order of magnitude above the transmitted pulse frequency, i.e. 54 kHz. The signals then were normalized prior to decomposition as follows:

$$\overline{S}(t) = \frac{S(t) - \mu}{max - min} \tag{7}$$

where μ, max, and min represent the mean, maximum and minimum values of the signal $S(t)$, respectively, and $\overline{S}(t)$ is the normalized signal. The ultrasonic signals were then decomposed into different numbers of IMFs, where the center frequencies of all IMFs are considered as DSFs. As such, K DSFs (center frequencies) can be derived by decomposing the signal into K IMFs. We hypothesize that over-decomposing the signal will produce IMFs with closer center frequencies, which will subsequently make the task of classification difficult. On the other hand, under-decomposing the signals will cause loss of information about the damage state of the specimens. Therefore, different numbers of decomposition and, thus, different numbers of features were used to obtain the optimum number of decomposition for each classification problem. Since the signals were passed through a lowpass filter prior to decomposition, the effect of the quadratic penalty term was neglected by setting $\tau = 0.1$. Furthermore, the tolerance parameter ϵ was set to 10^{-5} in this study. Figure 3 shows an example of a filtered and normalized ultrasonic signal decomposed into three IMFs along with their center frequencies. Figure 4 shows the Welch power spectral density (PSD) (see `pwelch` in MATLAB) of the IMFs corresponding to this decomposition. It has been mentioned in several researches that VMD, unlike EMD, does not suffer from the mode mixing phenomenon [48, 49]. However, the PSD plots of the obtained IMFs show some level of mode mixing in the obtained IMFs. However, applying the center frequency of IMFs as features can reduce the adverse effect of mode mixing on the classification problem.

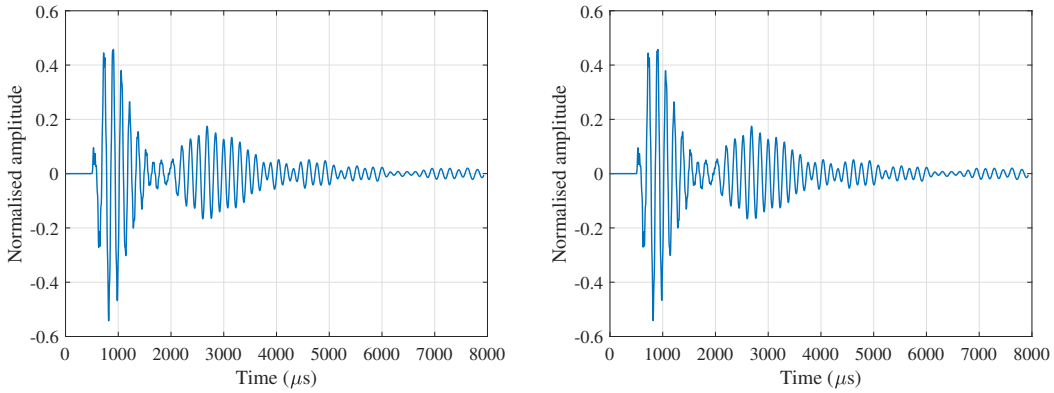

(a) $\overline{S}(t)$ (b) IMF$_1$, $\omega_1 = 0.0063$

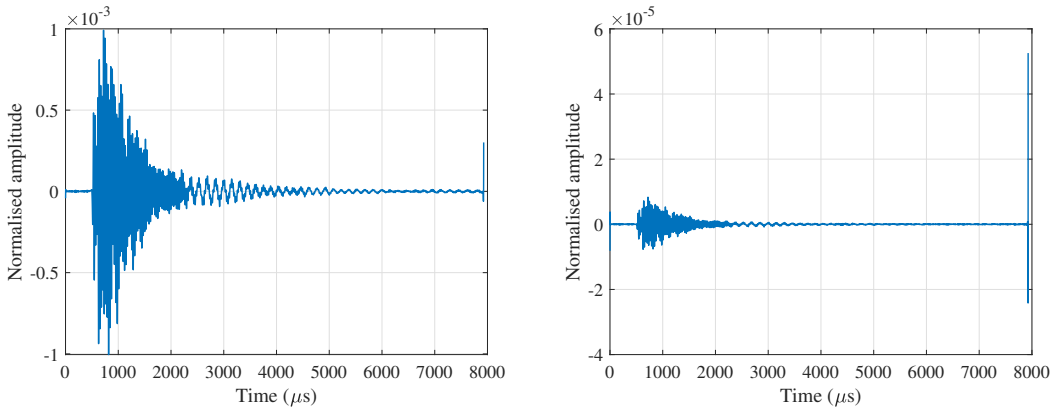

(c) IMF$_2$, $\omega_2 = 0.0345$ (d) IMF$_3$, $\omega_3 = 0.0854$

Figure 3: An example of filtered and normalised ultrasonic signal decomposed into three IMFs along with their center frequencies.

The derived features were then fed into a Gaussian naive Bayes classifier for classification in the MATLAB's machine learning and deep learning toolbox [50]. To that end, four different classification tasks were ran based on the prior knowledge about the type of wood and direction through which the tests were conducted. The tasks include: (1) soft wood in the radial direction, (2) soft wood in the tangential direction, (3) hard wood in the radial direction, and (4) hard wood in the tangential direction. Therefore, regarding the number of the tests conducted on each case (Table 1), there were 600 samples for each classification problem with 300 tests conducted on intact specimens, 150 tests conducted on specimens with small defects, and 150 tests conducted on specimens with large defects. Therefore, *a priori* probability was assigned to each class considering the proportional number of tests conducted for that class, specifically 0.5, 0.25, and 0.25 for intact, small damage, and large damage categories, respectively. A 10-fold cross-validation test was then ran on each classification problem.

Figure 5 displays the accuracy achieved for each classification task using different numbers

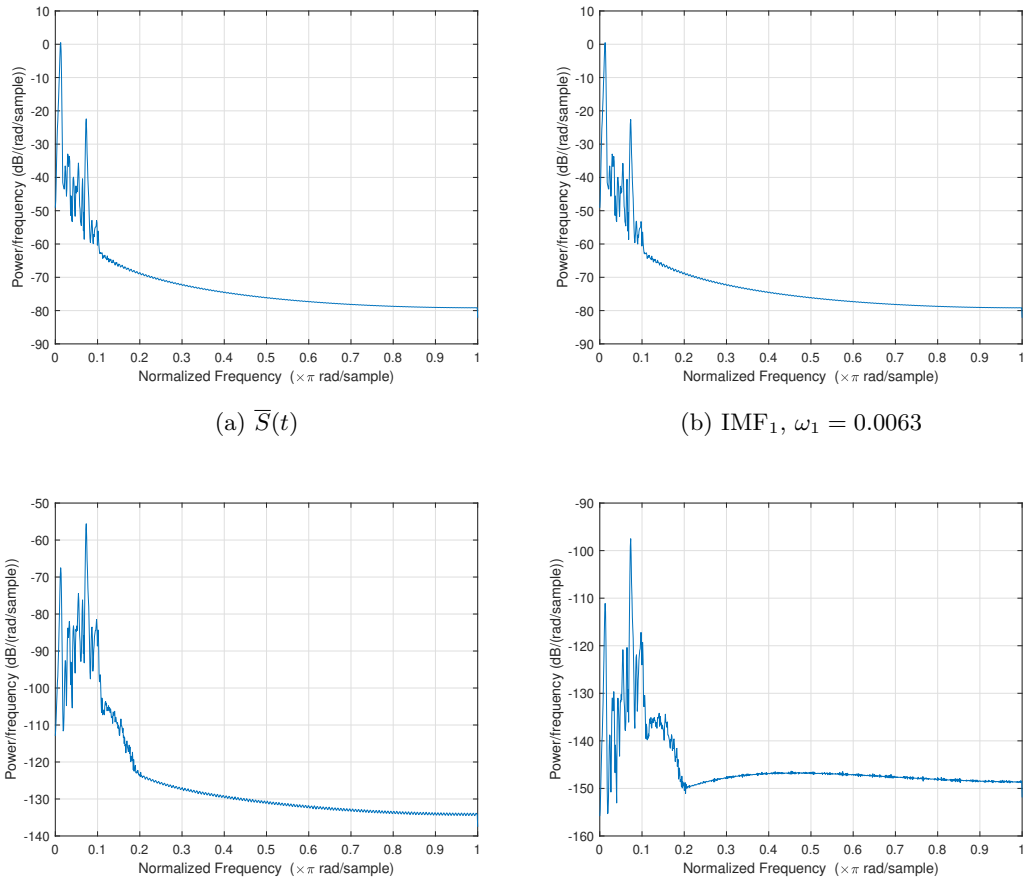

(a) $\overline{S}(t)$ (b) IMF_1, $\omega_1 = 0.0063$

(c) IMF_2, $\omega_2 = 0.0345$ (d) IMF_3, $\omega_3 = 0.0854$

Figure 4: Welch power spectral density of the original signal and its decomposed IMFS.

of decomposition (features). As can be seen from the figure, different results were obtained for different cases as the number of decomposition increased.

Regarding the accuracy obtained for marbau (hard wood) tested in the radial direction ($\mathrm{M_r}$), the best result of 83.33% accuracy was obtained using six features (Figure 5a). As previously hypothesized, the accuracy decreased when fewer or more features were used. However, as for marbau tested in the tangential direction ($\mathrm{M_t}$), the results are counter-intuitive as the trend completely reversed. Specifically, the best result, 100% accuracy, was achieved using only two (or three) features, plunged when using more features (up to seven), and then increased again thereafter (Figure 5b). Regarding the pine samples tested in the radial direction ($\mathrm{P_r}$), the best result, 99.5% accuracy, was achieved using three (or four) features (Figure 5c). Likewise, the accuracy decreased using fewer or more features (decomposition). A similar trend can be seen in the Figure 5d regarding the accuracy results obtained for the pine samples tested in the tangential direction ($\mathrm{P_t}$) where the best result of 71.17 % accuracy was achieved using three features (decomposition).

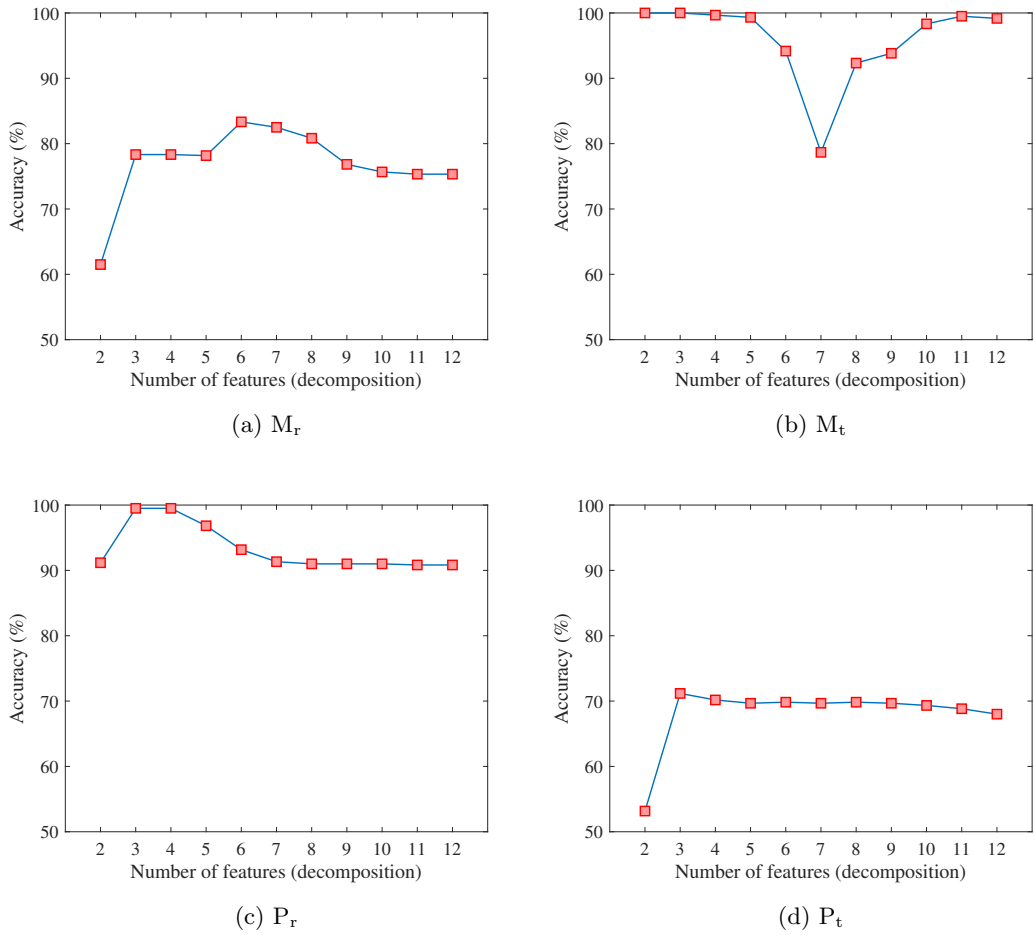

Figure 5: Calculated accuracy of classification problem run on each task after 10-fold cross-validation using center frequency of IMFs as features.

The results suggest that the best accuracy was achieved for M_t followed by P_r at 100% and 99.5%, respectively. However, the results of classification tasks ran on M_r and P_t are not satisfactory. Accordingly, the worst result was obtained for P_t at 71.17 % accuracy. The penultimate worst result was obtained for the classification task ran on M_r at 83.33 % accuracy. Therefore, we then shifted our attention on improving the results of classification problems of M_r and P_t.

Since a 10-fold cross-validation classification task was ran on each case, the confusion matrix obtained for each fold of cross-validation conducted on M_r and P_t is presented (Figures 6 and 7) to show how the classifier performs on each fold for these cases. Note that there are 60 data, $\frac{1}{10}$ of the entire dataset, used in each fold of cross-validation. While the classifier does not confuse any of the intact or small defect classes with other classes regarding M_r, it is clear that the classifier struggles with differentiating between the large defect class and other classes. As for P_t, however, the classifier confuses all classes with all others, whereby the worst results were

obtained for the large damage and the best results for the intact class. Therefore, we conclude that the classifier does not perform well using only the suggested features for these cases. Next, we propose new set of features to be extracted from ultrasonic signals using VMD, which were further employed in a classification problem regarding M_r and P_t.

5.2. New features for M_r and P_t

We propose two new features to be used for training classification tasks regarding M_r and P_t. The first feature is based on the idea proposed in [43]. As such, the maximum eigenvalue of the covariance matrix corresponding to the decomposed IMFs is used as a feature in here. Note that Empirical Mode Decomposition (EMD) was used in [43]. However, we exploit VMD in this paper.

Let $V_{K\times N}$ be the matrix of all IMFs stacked up in rows, where K is the number of IMFs and N is the length of each IMF equal to the number of elements in the original signal.[2] The proposed feature is then calculated as $max(eig(V \times V'))$. It was shown in [43] that this quantity is highly sensitive to damage in marbau wood but not in pine samples.[3] Therefore, we hypothesize that this feature will contribute to achieving better results when used for the damage classification of M_r using the Gaussian naive Bayes classifier. To test our hypothesis, the proposed feature was first used with the center frequencies of the best results from the previous section, i.e. 6 decompositions for M_r and 3 decompositions for P_t.

After applying 10-fold cross-validation on M_r cases, 100% accuracy was achieved using the new feature along with the optimum number of decompositions from the previous section, i.e. 6. However, as for P_t, only 67.83% accuracy was achieved, which is slightly less accurate than the previous results, i.e. 71.17%. This motivated us to apply the proposed feature with different numbers of decompositions regarding P_t.

Figure 8 reveals the accuracy obtained after 10-fold cross-validation applied to the classification problem regarding P_t using different numbers of decompositions (center frequencies) along with the new feature. As can be seen from the graph, the best result of 73.83% accuracy was obtained using 5 decompositions. However, no further improvement was achieved by increasing the number of decomposition (features). This demands a new set of features to be defined and employed for classifying P_t cases. As follows, we define a new set of features to be employed to this end.

[2]Note that the algorithm of EMD decomposes a signal into matrix $V_{N\times K}$, where N is equal to the length of the original signal and K is the number of IMFs.

[3]Note that no classification problem was solved in [43].

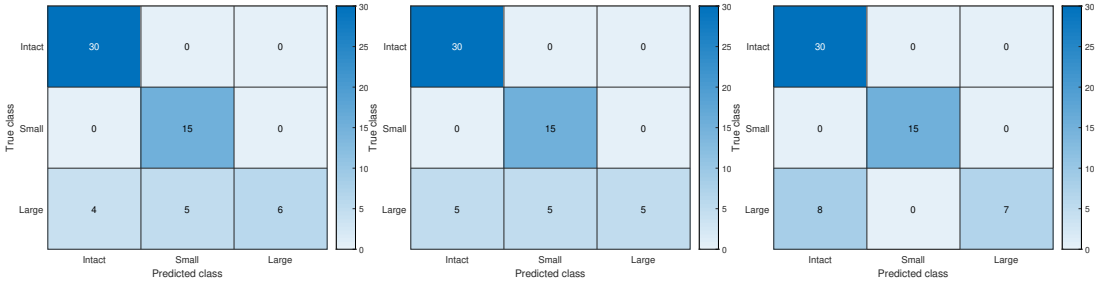

(a) 1^{st} fold

(b) 2^{nd} fold

(c) 3^{rd} fold

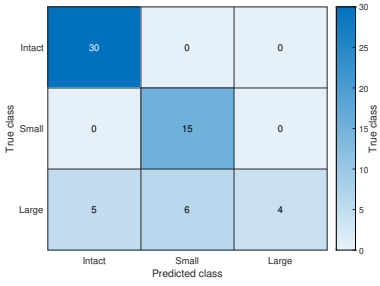

(d) 4^{th} fold

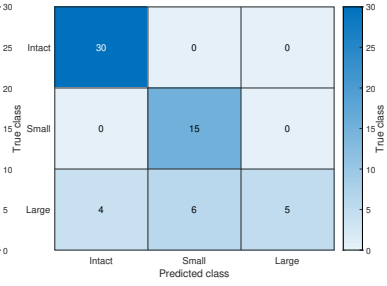

(e) 5^{th} fold

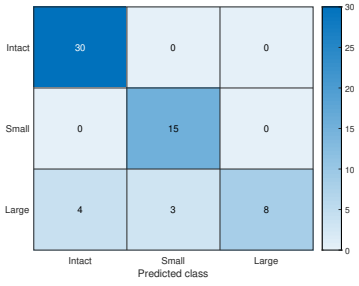

(f) 6^{th} fold

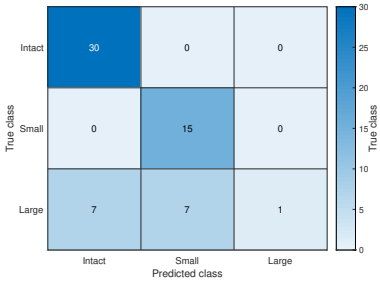

(g) 7^{th} fold

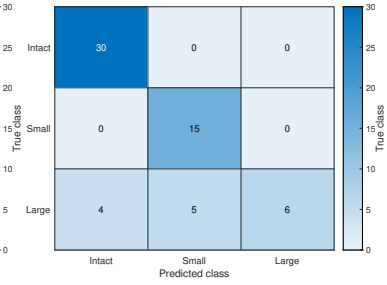

(h) 8^{th} fold

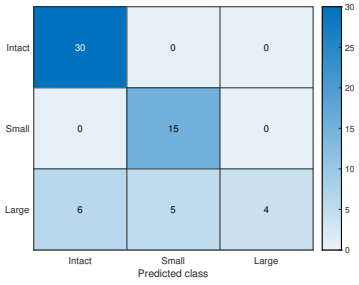

(i) 9^{th} fold

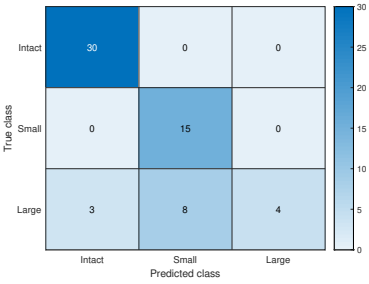

(j) 10^{th} fold

Figure 6: Confusion chart of classification problem run on each fold of 10-fold cross-validation regarding M_r.

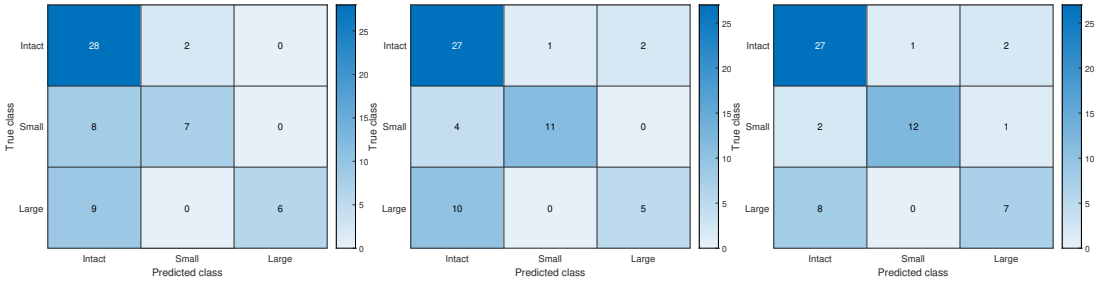

(a) 1^{st} fold

(b) 2^{nd} fold

(c) 3^{rd} fold

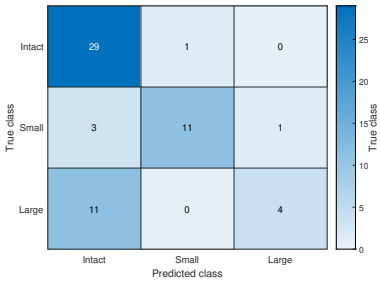

(d) 4^{th} fold

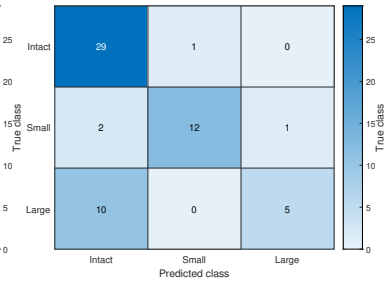

(e) 5^{th} fold

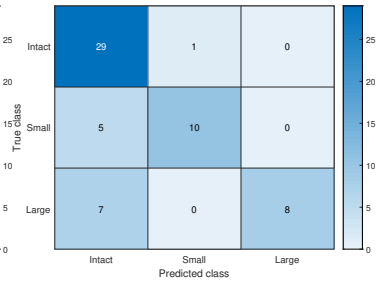

(f) 6^{th} fold

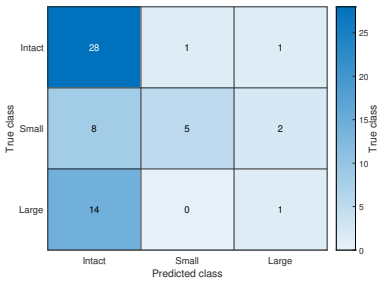

(g) 7^{th} fold

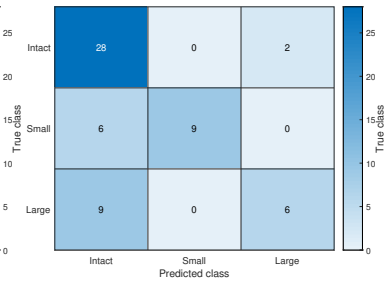

(h) 8^{th} fold

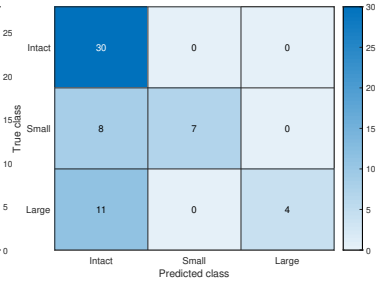

(i) 9^{th} fold

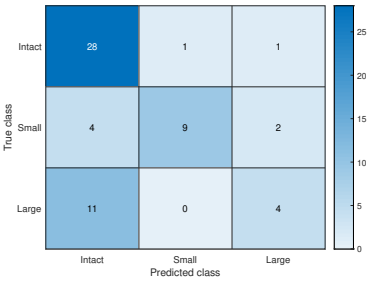

(j) 10^{th} fold

Figure 7: Confusion chart of classification problem run on each fold of 10-fold cross-validation regarding P_t.

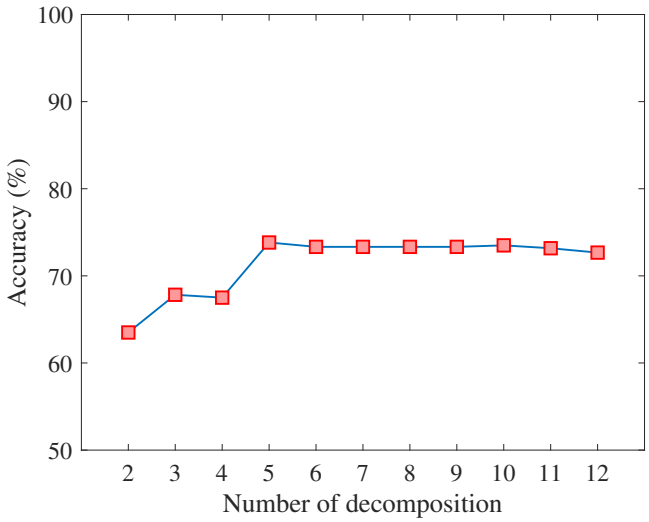

Figure 8: Accuracy obtained after 10-fold cross-validation applied to the classification problem using eigenvalue feature along with center frequencies of different number of IMFs regarding signal P_t.

Consider an ultrasonic signal decomposed into K IMFs. Then, the root mean square of instantaneous frequency (RMS_{IF}) of each IMF is taken as a feature. To that end, the Gabor analytical signal corresponding to an IMF is first constructed as follows [51]:

$$u_a(t) = u(t) + j\hat{u}(t), \tag{8}$$

where $u(t)$ and $\hat{u}(t)$ are the original IMF and its Hilbert transform [52], respectively. Next, the instantaneous frequency of IMF at time instant t is calculated as follows:

$$\omega(t) = \frac{\mathrm{d}}{\mathrm{d}t}\left(tan^{-1}\left(\frac{\hat{u(t)}}{u(t)}\right)\right), \tag{9}$$

The RMS_{IF} is then calculated as:

$$\mathrm{RMS}_{\mathrm{IF}}(t) = \sqrt{\frac{\sum_{i=1}^{n}\omega(t)^2}{n}}, \tag{10}$$

For K decomposition, K RMS_{IF} is obtained. We then employed these new features both individually and with the previous ones, i.e. the center frequencies of all IMFs, for solving the classification problem regarding P_t. As shown in Figure 9, regardless of the number of decomposition, a mixture of features almost always resulted in better outcomes than using each type of feature individually. Accordingly, the best result of 80.33% accuracy was obtained when using 3 decompositions. RMS_{IF} performed marginally better than mixed features only when 4 decompositions were used. It can also be seen from the graph that using RMS_{IF} individually performed better than center frequency features when the number of features was equal or less than 7. However, using a greater number of decomposition, i.e. greater than 7, and center frequency features alone improved the accuracy.

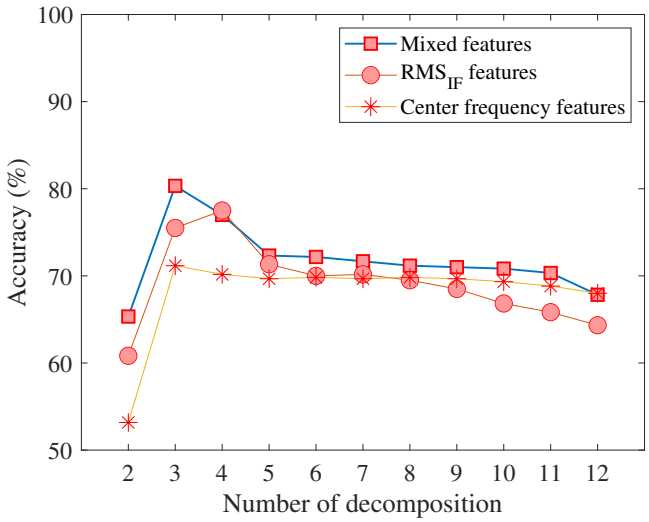

Figure 9: Accuracy obtained after 10-fold cross-validation applied to the classification problem using $\mathrm{RMS_{IF}}$, center frequency features and a mixture of them regarding $\mathrm{P_t}$.

Since the results thus far are not completely satisfactory, we then examined the mixed feature space of the center frequency and $\mathrm{RMS_{IF}}$ features to understand why the Gaussian naive Bayes is not able to classify $\mathrm{P_t}$ cases well. To that end, PCA was used to reduce the dimension of the feature space for visualisation purpose.

Figure 10 shows the landscape of the first principal component ($\mathrm{PC_1}$) versus the second principal component ($\mathrm{PC_2}$) corresponding to the mixed feature space of $\mathrm{RMS_{IF}}$ and center frequency features along with their Gaussian contours when the optimum number of 3 decompositions (6 features in total) was used. Figure 11 shows the scree plot corresponding to the application of the PCA to the mixed feature space. As such, $\mathrm{PC_1}$ and $\mathrm{PC_2}$ collectively capture 88.27% of the variance in the dataset. As can be seen from Figure 10, the reduced feature space regarding small and intact damage cases exhibited the greatest variability along the second principal axis, whereby the observations were relatively concentrated in a confined region. However, the observations regarding the large damage cases show the greatest variability along the first principal axis, where data points are concentrated in two separate regions with a gap between them. As such, using Gaussian distribution to work out the likelihood of these observations does not seem to be a good choice, which will consequently increase the difficulty of differentiating between the large damage cases and other cases, i.e. intact and small damage cases. As such, there is a considerable number of large damage cases confused with intact and or small damage cases. This suggests that a more complicated model needs to be considered for fitting the features to solve the classification problem. As such, the kernel naive Bayes model was used to address this issue.

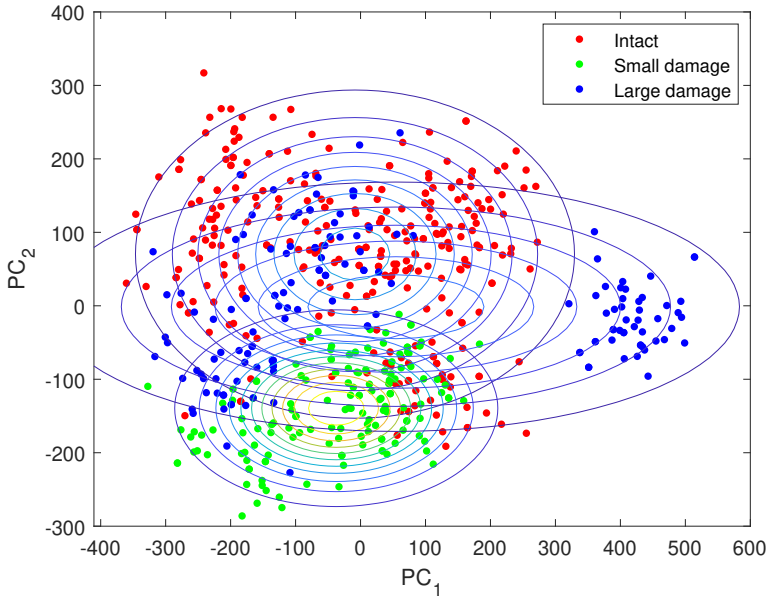

Figure 10: The landscape of the first principal component versus second principal component along with their Gaussian contours corresponding to the mixed feature space of $\mathrm{RMS_{IF}}$ and center frequencies of three decomposition of $\mathrm{P_t}$ ultrasonic signals.

5.3. Using kernel naive Bayes

So far, we have employed Gaussian naive Bayes, which uses Gaussian distribution model for the training set to calculate the likelihood of each feature in a given class. However, we have been only able to achieve 80.33% accuracy regarding the classification problem of $\mathrm{P_t}$. We demonstrated in the previous section that Gaussian naive Bayes is not a good model for calculating the Bayesian *a posteriori* likelihood of the features regarding $\mathrm{P_t}$, especially for the large damage cases. As such, in this section, we employed kernel naive Bayes to address this issue. To this end, the default of the normal kernel in MATLAB was employed. Also, the width for each class and predictor is selected by the classifier, automatically [50].

Figure 12 shows the accuracy results achieved after applying 10-fold cross-validation to the dataset corresponding to $\mathrm{P_t}$ using the kernel naive Bayes classifier. As can be seen from the figure, 100% accuracy was achieved using 3 decompositions when a mixture of center frequencies and $\mathrm{RMS_{IF}}$ features were used. The accuracy level dropped at 4 decompositions and then increased to 94.33% accuracy using 5 decompositions. However, as it is evident from the graph, the general trend of accuracy decreases when using a larger number of decomposition thereafter. This indicates that the kernel naive Bayes always performs better only when using the center frequency features and always performs worse using $\mathrm{RMS_{IF}}$ features alone. However, even using $\mathrm{RMS_{IF}}$ features alone, kernel naive Bayes can achieve an accuracy of 85.33%, which is still slightly better than 80.33% accuracy obtained by the Gaussian naive Bayes.

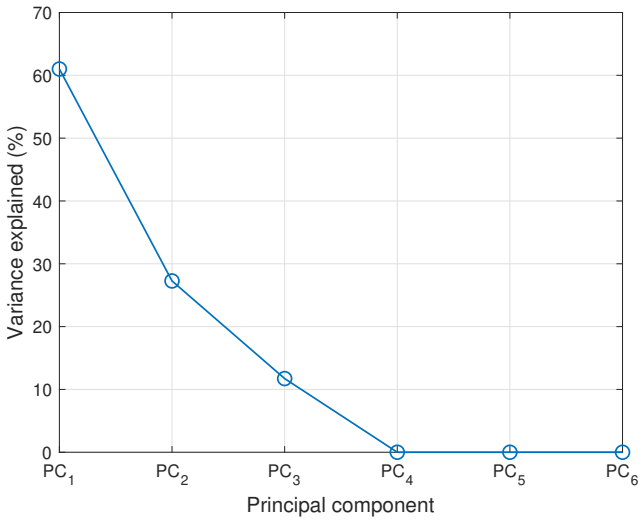

Figure 11: The scree plot of the application of the PCA to the mixed feature space of RMS_{IF} regarding P_t cases with the optimum number of the decomposition, i.e. 3.

5.4. Classification of mixed specimens based on their health state

So far, we have been studying each model individually to explore the nature of the wood material in the classification problems of this paper, and in order to find the best settings that work for even the hardest case, i.e. P_t. However, it is not always possible to have *a priori* knowledge about the type of the wood or the direction of the ultrasonic test with respect to the growth rings of wood. Therefore, in this section, all the specimens are mixed to classify them based on their health state only. As such, we solve the classification problem regardless of the type of the wood and the direction of the ultrasonic test.

There are thus 1200 cases of healthy specimens, 600 cases of small defects specimens, and 600 cases of large defects specimens, as can be seen from Table 1. The following settings are selected based on the results obtained so far:

1. The number of three decompositions is selected in the VMD settings as the optimum number of decomposition. As such, the center frequency and RMS_{IF} features were used either individually or combined to solve the classification problem of this section.
2. Both Gaussian and kernel naive Bayes were used to solve the problem for the purpose of comparison.

Table 2 shows the obtained results. As can be seen from the table, the best result of 93.6% 10-fold cross-validation accuracy was obtained when combined features were used in the kernel naive Bayes classifier. It can be noted that the penultimate best accuracy result was achieved at 85.8% when the mixed features were used in the Gaussian naive Bayes classifier, indicating that the selection of the type of features has a more significant effect on the penultimate best

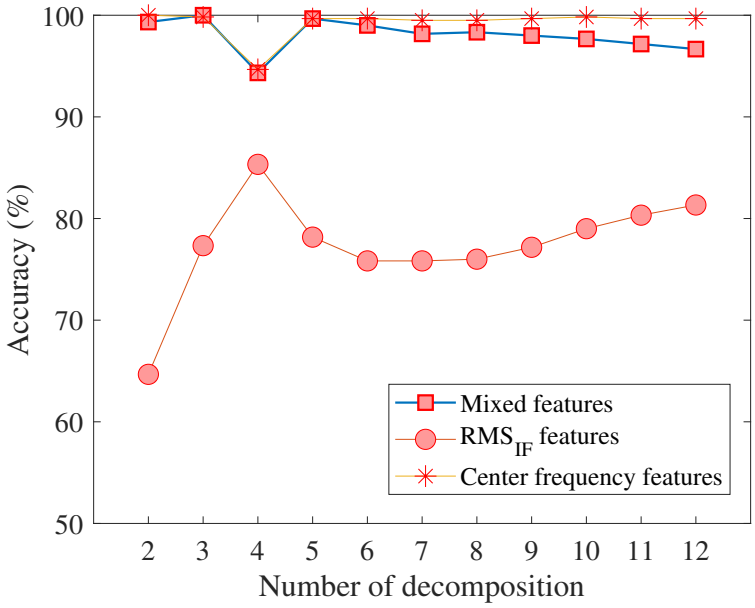

Figure 12: Accuracy obtained after 10-fold cross-validation applied to the classification problem using $\mathrm{RMS_{IF}}$, center frequency and a mixture of them using kernel naive Bayes.

Table 2: 10-fold cross-validation accuracy percentage of different naive Bayes classifiers using each of the center frequencies and $\mathrm{RMS_{IF}}$ classifiers and a mixture of both.

Classifier	**Center frequencies**	**$\mathbf{RMS_{IF}}$**	**Mixed**
Gaussian	73.3%	78%	85.8%
Kernel	83.4%	83.3%	93.6%

results than the type of the employed classifier in here. The worst accuracy result of 73.3% was achieved when the center frequency features were used in the Gaussian naive Bayes classifier.

6. Conclusions

A systematic classification problem of classifying hole-defects in two types of wood materials, i.e. marbau (hard wood) and pine (soft wood), has been presented and discussed. To that end, four different classification problems were solved based on the type of wood and direction through which the ultrasonic tests were conducted. First, VMD was used to decompose the ultrasonic signals into different numbers of IMFs, and the center frequencies of all IMFs were taken as features. Since VMD is a parametric decomposition algorithm, it is important that some parameters be set properly prior to decomposition. As such, it has been discussed how each parameter should be set for the purpose of this paper.

The results of the 10-fold cross-validation on each classification problem indicate that nearly 100% accuracy was obtained for $\mathrm{M_t}$ (100%) and $\mathrm{P_r}$ (99.5%) using the Gaussian naive Bayes

classifier. However, since the results were not as satisfactory for M_r and P_t, a new set of features was derived using VMD and then employed in the classification problems, as discussed in Section 5.2. The results were considerably improved using the Gaussian naive Bayes classifier, which achieved 100% accuracy on M_r cases. Although the results improved in the case of P_t, an accuracy of more than 80.33% could not be obtained.

The Gaussian naive Bayes classifier uses a normal distribution model for the entire training set to calculate *a posteriori* Bayesian. Since, it was found that this classifier fails to achieve perfect results regarding P_t using the proposed features, we employed kernel naive Bayes classifier to address this issue. The results show that 100% accuracy can be achieved after employing the kernel naive Bayes using either the center frequency features alone or with the RMS_{IF} features.

Next, the classification problem of the wood specimens regardless of the type of wood and the direction of the ultrasonic test with respect to the growth rings of wood was solved. 93.6% 10-fold cross-validation accuracy was achieved following choosing the settings distinguished best from solving the hardest classification problem of P_t cases. As such, we conclude that a mixture of center frequencies and RMS_{IF} features along with the kernel naive Bayes classifier are the best settings for solving the classification problem of wood specimens based on their health state only. The number of three decompositions is also recommended as the optimum number of decompositions. Moreover, the complementary RMS_{IF} features have helped with avoiding bias in the training process of the machine learning algorithm. Based on the obtained results, the authors recommend that the number of decompositions should not exceed six, as it may bring about losing information due to the over-decomposition of the signals.

The possibility of using naive Bayes classifiers for supervised classification of contact ultrasonic test results, conducted on different types of wooden specimens with artificial defects, has been investigated in this paper. Accordingly, in order to facilitate obtaining accurate labels to be assigned to each test result, artificial defects were implemented on the specimens. These sorts of damage have been studied by other researchers as well (for example see [12, 23, 53]). The main reason for studying wood hole-defects is that these sorts of damage are aimed to mimic defects that are often seen in standing trees when the trees are not pruned in time. It is, however, possible to label specimens based on other types of imperfections such as those caused by fungi and termite attacks, and weathering. To this end, other techniques such as using a Resistograph [54] needs to be employed to make it possible to label the obtained dataset more accurately. Since the results of the current study are quite promising, future work can be dedicated to solving such a more realistic problem.

References

[1] N. G. Bingel, Cost saving benefits of wood structure maintenance [for power overhead lines], in: Proceedings of ESMO'95-1995 IEEE 7th International Conference on Transmission and Distribution Construction, Operation and Live-Line Maintenance, IEEE, 1995, pp. 11–16.

[2] J. Li, U. Dackermann, M. Subhani, R&D of NDTs for timber utility poles in service-challenges and applications (extension for bridge sub-structures and wharf structures), in: Proceedings of the Workshop on Civil Structural Health Monitoring (CSHM-4), Bundesanstalt für Materialforschung und -prüfung (BAM), Berlin, Germany, 2012, pp. 6–8.

[3] S. Bandara, P. Rajeev, E. Gad, B. Sriskantharajah, I. Flatley, Damage detection of in service timber poles using Hilbert-Huang transform, NDT & E International (2019) 102141.

[4] Y. Yu, U. Dackermann, J. Li, E. Niederleithinger, Wavelet packet energy–based damage identification of wood utility poles using support vector machine multi-classifier and evidence theory, Structural Health Monitoring 18 (1) (2019) 123–142.

[5] D. W. Green, J. E. Winandy, D. E. Kretschmann, Mechanical properties of wood. Wood handbook : wood as an engineering material (Chapter 4), Vol. GTR-113, Madison, WI : USDA Forest Service, 1999.

[6] EN 408:2010+A1:2012 – Timber structures, Structural timber and glued laminated timber, Determination of some physical and mechanical properties, Standard, European Standards (2010).

[7] M. H. Ramage, H. Burridge, M. Busse-Wicher, G. Fereday, T. Reynolds, D. U. Shah, G. Wu, L. Yu, P. Fleming, D. Densley-Tingley, et al., The wood from the trees: The use of timber in construction, Renewable and Sustainable Energy Reviews 68 (2017) 333–359.

[8] U. Dackermann, R. Elsener, J. Li, K. Crews, A comparative study of using static and ultrasonic material testing methods to determine the anisotropic material properties of wood, Construction and Building Materials 102 (2016) 963–976.

[9] L. Yu, Y. Liang, Y. Zhang, J. Cao, Mechanical properties of wood materials using near-infrared spectroscopy based on correlation local embedding and partial least-squares, Journal of Forestry Research 31 (3) (2020) 1053–1060.

[10] Y. Yang, X. Zhou, Y. Liu, Z. Hu, F. Ding, Wood defect detection based on depth extreme learning machine, Applied Sciences 10 (21) (2020) 7488.

[11] F. Pantelić, M. Mijić, D. Šumarac Pavlović, D. Ridley-Ellis, D. Dudeš, Analysis of a wooden specimen's mechanical properties through acoustic measurements in the very near field, The Journal of the Acoustical Society of America 147 (4) (2020) EL320–EL325.

[12] M. Mori, M. Hasegawa, J.-C. Yoo, S.-G. Kang, J. Matsumura, Nondestructive evaluation of bending strength of wood with artificial holes by employing air-coupled ultrasonics, Construction and Building Materials 110 (2016) 24–31.

[13] T. Palander, J. Eronen, K. Kärhä, H. Ovaskainen, Development of a wood damage monitoring system for mechanized harvesting, Annals of Forest Research 61 (2) (2018) 243–258.

[14] U. Dackermann, B. Skinner, J. Li, Guided wave–based condition assessment of in situ timber utility poles using machine learning algorithms, Structural Health Monitoring 13 (4) (2014) 374–388.

[15] Y. Yu, M. Subhani, A. N. Hoshyar, J. Li, H. Li, Automated health condition diagnosis of in situ wood utility poles using an intelligent non-destructive evaluation (nde) framework, International Journal of Structural Stability and Dynamics (2020).

[16] Y. Lee, M. Mahoor, W. Hall, A 2d numerical model of ultrasonic wave propagation in wooden utility poles using embedded waveguide excitation technique, Wood and Fiber Science 52 (1) (2020) 87–101.

[17] B. Sriskantharajah, E. Gad, S. Bandara, P. Rajeev, I. Flatley, Condition assessment tool for timber utility poles using stress wave propagation technique, Nondestructive Testing and Evaluation 36 (3) (2021) 336–356.

[18] B. İpekoğlu, An architectural evaluation method for conservation of traditional dwellings, Building and environment 41 (3) (2006) 386–394.

[19] H. Cruz, D. Yeomans, E. Tsakanika, N. Macchioni, A. Jorissen, M. Touza, M. Mannucci, P. B. Lourenço, Guidelines for on-site assessment of historic timber structures, International Journal of Architectural Heritage 9 (3) (2015) 277–289.

[20] M. M. Conde, C. R. Liñán, P. R. de Hita, Use of ultrasound as a nondestructive evaluation technique for sustainable interventions on wooden structures, Building and Environment 82 (2014) 247–257.

[21] M. Van Leeuwen, T. Hilker, N. C. Coops, G. Frazer, M. A. Wulder, G. J. Newnham, D. S. Culvenor, Assessment of standing wood and fiber quality using ground and airborne laser scanning: a review, Forest Ecology and Management 261 (9) (2011) 1467–1478.

[22] Q. Zhao, S. Yu, F. Zhao, L. Tian, Z. Zhao, Comparison of machine learning algorithms for forest parameter estimations and application for forest quality assessments, Forest Ecology and Management 434 (2019) 224–234.

[23] H. Yang, L. Yu, Feature extraction of wood-hole defects using wavelet-based ultrasonic testing, Journal of forestry research 28 (2) (2017) 395–402.

[24] W. Li, J. Van den Bulcke, D. Mannes, E. Lehmann, I. De Windt, M. Dierick, J. Van Acker, Impact of internal structure on water-resistance of plywood studied using neutron radiography and X-ray tomography, Construction and Building Materials 73 (2014) 171–179.

[25] G. López, L. A. Basterra, L. Acuña, Estimation of wood density using infrared thermography, Construction and Building Materials 42 (2013) 29–32.

[26] E. Blomme, D. Bulcaen, F. Declercq, Air-coupled ultrasonic nde: experiments in the frequency range 750 kHz–2 MHz, NDT & E International 35 (7) (2002) 417–426.

[27] A. C. Senalik, G. Schueneman, R. J. Ross, Ultrasonic-based nondestructive evaluation methods for wood: a primer and historical review, USDA Forest Service, Forest Products Laboratory, General Technical Report, FPL-GTR-235, 2014; 36 p. 235 (2014) 1–36.

[28] T. Goto, Y. Tomikawa, S. Nakayama, T. Furuno, Changes of propagation velocity of ultrasonic waves and partial compression strength of decay-treated woods relationship between decrease of propagation velocity of ultrasonic waves and remaining strength, Mokuzai Gakkaishi 57 (6) (2011) 359–369.

[29] S. Lee, S.-J. Lee, J. S. Lee, K.-B. Kim, J.-J. Lee, H. Yeo, Basic study on nondestructive evaluation of artificial deterioration of a wooden rafter by ultrasonic measurement, Journal of Wood Science 57 (5) (2011) 387–394.

[30] F. Tallavo, G. Cascante, M. D. Pandey, A novel methodology for condition assessment of wood poles using ultrasonic testing, NDT & E International 52 (2012) 149–156.

[31] T. Mori, Y. Yanase, K. Tanaka, K. Kawano, Y. Noda, M. Mori, H. Kurisaki, K. Komatsu, Evaluation of compression and bending strength properties of wood damaged from biodeterioration, Journal of the Society of Materials Science, Japan 62 (4) (2013) 280–285.

[32] S.-J. Lee, S. Lee, S.-J. Pang, C.-K. Kim, K.-M. Kim, K.-B. Kim, J.-J. Lee, Indirect detection of internal defects in wooden rafter with ultrasound, Journal of the Korean Wood Science and Technology 41 (2) (2013) 164–172.

[33] A. Ettelaei, M. Layeghi, H. Z. Hosseinabadi, G. Ebrahimi, Prediction of modulus of elasticity of poplar wood using ultrasonic technique by applying empirical correction factors, Measurement 135 (2019) 392–399.

[34] S. Lee, S.-J. Lee, J. S. Lee, K.-B. Kim, J.-J. Lee, H. Yeo, Basic study on nondestructive evaluation of artificial deterioration of a wooden rafter by ultrasonic measurement, Journal of wood science 57 (5) (2011) 387–394.

[35] L. Reinprecht, M. Pánek, Ultrasonic technique for evaluation of bio-defects in wood: Part 1–influence of the position, extent and degree of internal artificial rots, International Wood Products Journal 3 (2) (2012) 107–115.

[36] M. Hirao, H. Ogi, EMATs for science and industry: noncontacting ultrasonic measurements, Springer Science & Business Media, 2013.

[37] L. Drain, Laser ultrasonics techniques and applications, Routledge, 2019.

[38] W. Grandia, C. Fortunko, Nde applications of air-coupled ultrasonic transducers, in: 1995 IEEE Ultrasonics Symposium. Proceedings. An International Symposium, Vol. 1, IEEE, 1995, pp. 697–709.

[39] Y. Fang, L. Lin, H. Feng, Z. Lu, G. W. Emms, Review of the use of air-coupled ultrasonic technologies for nondestructive testing of wood and wood products, Computers and electronics in agriculture 137 (2017) 79–87.

[40] D. Chimenti, Review of air-coupled ultrasonic materials characterization, Ultrasonics 54 (7) (2014) 1804–1816.

[41] T. Marhenke, J. Neuenschwander, R. Furrer, J. Twiefel, J. Hasener, P. Niemz, S. J. Sanabria, Modeling of delamination detection utilizing air-coupled ultrasound in wood-based composites, NDT & E International 99 (2018) 1–12.

[42] Operating instructions, pundit pl-200, Proceq SA (2013) p16.

[43] M. Mousavi, M. S. Taskhiri, D. Holloway, J. Olivier, P. Turner, Feature extraction of wood-hole defects using empirical mode decomposition of ultrasonic signals, NDT & E International (2020) 102282.

[44] K. Dragomiretskiy, D. Zosso, Variational mode decomposition, IEEE Transactions on Signal Processing 62 (3) (2014) 531–544.

[45] D. Zosso, Variational mode decomposition, matlab central file exchange (Retrieved August 27, 2020).
URL https://www.mathworks.com/matlabcentral/fileexchange/44765-variational-mode-decomposition

[46] Y. Wang, R. Markert, J. Xiang, W. Zheng, Research on variational mode decomposition and its application in detecting rub-impact fault of the rotor system, Mechanical Systems and Signal Processing 60 (2015) 243–251.

[47] I. Rish, et al., An empirical study of the naive bayes classifier, in: IJCAI 2001 workshop on empirical methods in artificial intelligence, Vol. 3, 2001, pp. 41–46.

[48] Z. Feng, D. Zhang, M. J. Zuo, Adaptive mode decomposition methods and their applications in signal analysis for machinery fault diagnosis: a review with examples, IEEE access 5 (2017) 24301–24331.

[49] A. Aghnaiya, Y. Dalveren, A. Kara, On the performance of variational mode decomposition-based radio frequency fingerprinting of bluetooth devices, Sensors 20 (6) (2020) 1704.

[50] Matlab Machine Learning and Deep Learning Toolbox, The MathWorks, Natick, MA, USA (2020).

[51] D. Gabor, Theory of communication. part 1: The analysis of information, Journal of the Institution of Electrical Engineers-Part III: Radio and Communication Engineering 93 (26) (1946) 429–441.

[52] M. Mousavi, D. Holloway, J. Olivier, A. H. Gandomi, Beam damage detection using synchronisation of peaks in instantaneous frequency and amplitude of vibration data, Measurement (2020) 108297.

[53] Y. Huimin, W. Lihai, Nondestructive testing of wood hole defect by ultrasonic spectrum analysis, JOURNAL-NORTHEAST FORESTRY UNIVERSITY-CHINESE EDITION-35 (8) (2007) 30.

[54] I. Fundova, T. Funda, H. X. Wu, Non-destructive wood density assessment of scots pine (pinus sylvestris l.) using resistograph and pilodyn, PLoS One 13 (9) (2018) e0204518.